Factorial Design Applied to CFD

Michel J. Cervantes
Michel.Cervantes@ltu.se

T. Fredrik Engström
Fredrik.Engstrom@ltu.se

Division of Fluid Mechanics, Luleå University of Technology, SE-97187 Luleå, Sweden

Factorial design, a statistical method widely used for experiments, and its application to CFD are discussed. The aim is to propose a systematic, objective, and quantitative method for engineers to design a set of simulations in order to evaluate main and joint effects of input parameters on the numerical solution. The input parameters may be experimental uncertainty on boundary conditions, unknown boundary conditions, grid, differencing schemes, and turbulence models. The complex flow of the Turbine-99 test case, a hydropower draft tube flow, is used to illustrate the method, where four factors are chosen to perform a 2^4 factorial design. The radial velocity at the inlet (not measured) is shown to have an important influence on the pressure recovery (7%) and the energy loss factor (49%). [DOI: 10.1115/1.1792277]

1 Introduction

The use of computer simulations to predict turbulent flows in complex geometries instead of model, or full scale, experiments can substantially decrease the cost of a project and still increase the knowledge of the flow problem. It makes such an approach attractive to the industry. Even if widely used, computational fluid dynamics (CFD) is not fully trusted by industry due to difficulties of obtaining reliable results. Until now, most academic work has been directed towards the validation of particular codes and turbulence models in simplified geometries [1]. Recently, more effort has been dedicated to compile the knowledge of all parts of CFD and its application in order to guide the usage of CFD as an engineering tool and thus improve the quality of the simulations. Members from both industry and the academic world work in this direction in the QNET-CFD network [1] and the ERCOFTAC Special Interest Group Quality and Trust for the Industrial Application of CFD [2]. The latter recently published the *Best Practice Guidelines* for industrial CFD users, edited by Casey and Wintergerste [3].

The lack of reliability of CFD in industrial applications is due to the discrepancy between simulated and experimental results and the difficulty to identify the sources of error. Turbulence models and grid errors are often discussed. It is true that ''simple turbulence models'' often are used for industrial simulations, which have difficulties in reproducing complex industrial flows. Also, the actual computational power makes grid-independent solutions difficult to achieve. Furthermore, the fluid engineers using CFD face a difficult task with a multitude of inputs and assumptions necessary to simulate a problem. These difficulties also contribute to making the results uncertain, which may force the engineer to stop at a qualitative instead of a quantitative assessment of the results. However, with the computational power now available, several test cases can be investigated, thus allowing a sensitivity analysis of the input parameters as recommended by the *Best Practice Guidelines* [3]. Several authors have already used such an approach, but there seems not to have been a systematic approach to plan and quantify the results. A complicating factor in such studies is that interaction between several factors may not be detected by varying one parameter at a time. Therefore, a systematic method to evaluate the simultaneous effects of several parameters on the numerical solution is necessary for engineers to get a quantitative ground for flow design.

The input parameters in CFD are numerous. They may be divided into three main groups: *flow modeling*, *numerics*, and *implementation*. The *flow modeling* embraces the mathematical modeling of the flow as well as the boundary conditions. The mathematical modeling involves several approximations that differ from one model to another, e.g. two-equation and second-moment closure turbulence models have different levels of approximation. Large eddy simulations (LES) begin to appear in commercial codes and represent yet another level. The boundary conditions may be experimental data such as velocity profiles, flow rates, pressures, wall roughness, etc. However, some or all boundary conditions must often be estimated, due to the technical difficulties and/or financial cost to measure them. Also, even in cases where experimental data are available, it has to be adapted for the computations, which often calls for further processing such as smoothing and extrapolation. The *numerics* involves the grid, the discretization method, the numerical scheme(s), the solver, and the convergence criteria. Important issues are grid independence, discretization, and iterative errors. There are methods to estimate these errors. For instance, Bergström and Gebart [4] used Richardson extrapolation with curve fitting to investigate the discretization error. The *implementation* is concerned with the generation of the CFD code. The user cannot always influence this issue since the code is normally developed by others. However, comparison between different codes may be performed as done by Iaccarino [5], who pointed out the different implementations of the same turbulence model in three commercial codes.

The complexity of CFD may be compared to industrial processes, such as the chemical industry, which contain many parameters whose influence and interaction are seldom clearly understood. A standard approach to analyze such complex processes is *factorial design*, a statistical method that quantifies the influence of the parameters. The present work presents the application of factorial design to CFD and a complex engineering flow, the Turbine-99 draft tube test case, is used to illustrate the method. The influence of four input parameters are evaluated on engineering quantities such as pressure recovery and energy loss factor. The results and a discussion are followed by the conclusions.

2 Factorial Design

Factorial design is a statistical method for experimental design. The main areas of use are process troubleshooting, development and optimization. A short description of the method is presented. Further information may be found in the book by Box, Hunter, and Hunter [6].

In this method, the factors influencing a process are varied in a certain pattern leading to a set of experimental runs. The influence of one factor (main effect) and the interaction of different factors (joint effect) on one or more representative quantities of the process are evaluated. Such a quantity may be the yield in a production process or an objective function in an optimization. It is important to note that interaction between several factors may not be detected by varying only one factor at a time. Potentially, all input parameters may be subject for investigation. A successful factorial design depends on the choice of the key factors, e.g., the most

Contributed by the Fluids Engineering Division for publication in the JOURNAL OF FLUIDS ENGINEERING. Manuscript received by the Fluids Engineering Division August 21, 2002; revised manuscript received May 12, 2004. Associate Editor: W. W. Copenhaver.

influencing factors for an optimization. If k factors are chosen, and each factor is tested at n levels (values), the design is called a n^k factorial design, since each experimental trial has n^k runs. Therefore, n^k statistics can be calculated; one average, k main effects, $\binom{k}{2}$ 2-factor interactions, . . . , and one k-factor interaction. The interpretation of a variable's main effect is made individually only if there is no evidence of interaction with other variables. Generally, for a large number of factors, the higher-order interactions may be neglected, since they are mainly due to experimental noise. Instead, they may be used to estimate the error level of an effect and thereby the significance of that effect. Replicated runs may also be performed for error analysis.

A two-level design is generally used as a first step in the analysis of a process where each parameter is assigned either a ''low'' or a ''high'' value. The main and joint effects are calculated as the difference between the mean of the high levels and the mean of the low levels. For joint effects, an even number of low levels for the interacting factors contribute to the high level value of the effect and an odd number of low levels contribute to the low level value. Further investigation of the process may be done by the introduction of a new factor or by the addition of new levels for one or more factors to detect nonlinear effects, as they are not detected by a two-level design.

In order to avoid redundance when several factors are chosen, *fractional factorial design* may be used to reduce the number of runs by a factor two. For instance, in a 2^5 factorial design, interactions between three factors or more may not be considered important, thus reducing the number of runs by two, from 2^5 to 2^4. By choosing the reduced number of runs after a certain pattern, an optimum resolution for the interactions may be found. Reducing the number of runs confounds disregarded higher-order interactions with assumed significant effects and interactions. For the reduced 2^5 design, main effects are confounded with fourth-order interactions, second-order interactions are confounded with third-order interactions and the mean value is confounded with the fifth-order interaction. The reduced number of runs of fractional factorial designs is advantageous in CFD, since complex industrial turbulent flow simulations may require several hours or days to converge and generally have several unknown input parameters.

The application of factorial design to CFD differs from its application to industrial processes since a simulation will yield exactly the same result over and over again, if the same residual is reached and machine precision error can be neglected. Therefore, a *standard error analysis* based on replicated runs is not possible in CFD. Furthermore, higher-order interactions are significant for fully converged solutions, since there is no random variation in the inputs of CFD, i.e., no noise. However, if a simulation is not fully converged, the quantity under evaluation may contain an iterative error. It sets a threshold in the significance of the different effects.

The identification of the key factors and their levels represents the main task for success with factorial design applied to CFD. The levels may be specified by experimental uncertainties in the case of a measured boundary condition. For unknown parameter values, a preliminary study may be necessary or assumptions for the appropriate upper and lower levels may be made. Compared to a single value, two levels give both an average and an indication of the sensitivity. Since the factors in factorial design may also be categorical variables, any input in CFD such as the turbulence model, differencing scheme, and computational grid may also be investigated with this approach.

The simulation of the complex flow encountered in a hydropower draft tube is treated to illustrate the method. The case is of great interest since two workshops on this flow have been organized and results are available. Therefore, comparison can be made between the result of the workshops and the result of the factorial design.

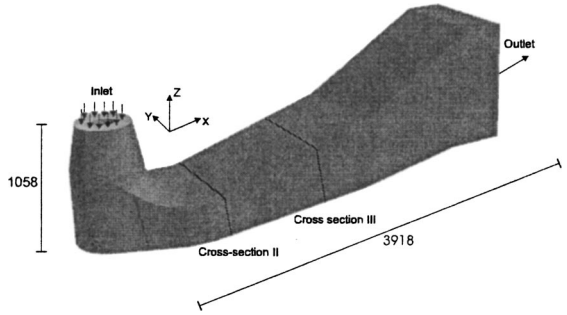

Fig. 1 CAD drawing of the Höllefors draft tube, dimensions in millimeters

3 The Turbine-99 Benchmark

Luleå University of Technology and Vattenfall Utveckling AB, Sweden, jointly organized the two Turbine-99 IAHR/ERCOFTAC Workshops in 1999 [7] and 2001 [8]. The aim was to determine the state of the art in CFD simulations of hydropower draft tube flows.

The draft tube follows immediately after the runner. The function of the draft tube is to convert the kinetic energy of the fluid leaving the runner into pressure energy with a minimum of losses. Modern draft tubes are composed from the inlet to the outlet of a conical diffuser, an elbow, and a straight asymmetric diffuser. A cone is attached below the runner to avoid a large separation region, which gives an annular inlet. Figure 1 shows the Höllefors draft tube model (1:11) used for the workshop; the inlet outer diameter is 472 mm and the inner diameter is 196 mm.

Draft tube flows are challenging for the CFD community due to the different phenomena that appear: swirling flow in straight and curved diffusers, separation, unsteadiness, impingement, and turbulence. It also presents an interesting engineering challenge since major hydropower installations in Sweden were built in the 1950s and will soon be refurbished [9]. In low head power plants, the draft tube is responsible for up to 50% of the total losses at high loads. Although hydropower plants are already highly efficient, up to 95%, a small increase in efficiency would correspond to a great value for the hydropower companies.

For the first workshop, the organizers provided the geometry of the draft tube model, as well as an extensive set of experimental data for the inlet boundary conditions measured in a 1:11 draft tube model at Vattenfall Utveckling AB [7] (Fig. 1). Some data at the inlet could not be measured, such as the radial velocity, some of the Reynolds stresses, and the turbulence (dissipation) length scale. The periodic fluctuations arising from the blade passages and the turbulent fluctuations in the measurements were chosen by the organizers to contribute to the steady turbulent intensities. The grid and the turbulence model were not disclosed to the participants.

The results of the pressure recovery obtained by the different participants at the first workshop presented a significant scatter, $\pm 45\%$ (see Fig. 2). The results of the second workshop will be commented on later in the discussion. The scatter is explained by the different assumptions for the boundary conditions as well as the different codes, grids, and turbulence models used by the participants. Several participants undertook a sensitivity analysis for some boundary conditions. For instance, Page and Giroux [7] investigated the inlet radial velocity and Bergström [7] the grid. This kind of analysis will be systemized here with factorial design.

3.1 Choice of Factors. The choice of the factors focused on the lack of information about the boundary conditions. Therefore, the radial velocity and the turbulence length scale at the inlet and also the surface roughness on the walls were chosen. The Reynolds stress could also have been a factor. However, the difficulty

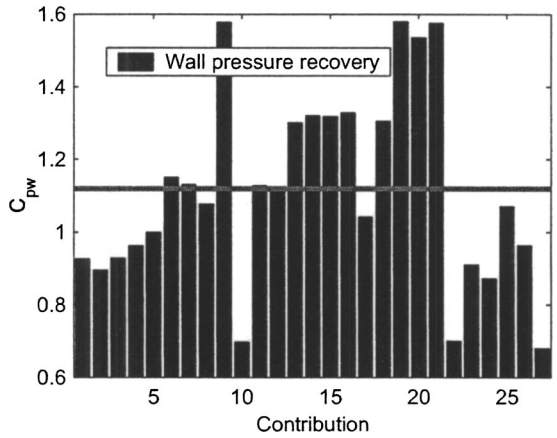

Fig. 2 Pressure recovery obtained at the first Turbine-99 Workshop. The line represents the experimental value 1.12.

to assign relevant levels is far from trivial in such a flow. The variety of grids present at the Turbine-99 workshop and the difficulty to obtain grid-independent solutions makes the grid an interesting factor.

A full factorial design at two levels was used. Thus, $2^4=16$ runs were performed. The different runs are presented in Table 1, where TLS, RV, and SR stand, respectively, for turbulence length scale, radial velocity, and surface roughness. The high and low levels are represented by + and a −, respectively.

3.1.1 Turbulence Length Scale. There are no experimental data on the turbulence length scale. According to Casey and Wintergerste [3], the turbulence length scale should be 1–10 % of the hydraulic diameter for internal flows. The hydraulic diameter at the inlet of the draft tube is defined as

$$D_H=\frac{4A}{P}=\frac{4\pi(R_{\text{wall}}^2-R_{\text{cone}}^2)}{2\pi(R_{\text{wall}}+R_{\text{cone}})}=2(R_{\text{wall}}-R_{\text{cone}}),$$

where A is the area of the cross section and P the wetted perimeter. The hydraulic diameter here is $D_H=0.28$ m and the corresponding turbulence length scale l ranges from 2.8 to 28 mm. The values 5 and 100 mm have been used as test values. The value of 100 mm was given by the organizers of the second Turbine-99 workshop.

The turbulence or dissipation length scale defines the inlet boundary condition for the dissipation rate ϵ of the turbulent kinetic energy k. The inlet boundary condition for k is estimated from the measured rms velocities. The dissipation rate is set to

$$\epsilon=\frac{k_{\text{inlet}}^{3/2}}{l}$$

where k_{inlet} is the turbulent kinetic energy at the inlet. A low value of the turbulence length scale corresponds to a high level of dissipation and vice versa.

3.1.2 Radial Velocity Profile. The radial velocity profile at the inlet was not measured. For the second workshop, the organizers assigned a velocity profile based on the assumption that the flow is attached to the walls at the inlet. The inlet has an annular cross section with the diffuser cone of the draft tube on the outside and the runner cone on the inside. The assumption of attached flow was used by Bergström and Gebart [4] at the first workshop and further confirmed by Nilsson [8] at the second workshop by a numerical investigation of the corresponding runner flow. In this case, the radial velocity is determined by the following relation:

$$u_{\text{radial}}=u_{\text{axial}}\tan(\theta),$$
$$\theta=\theta_{\text{cone}}+\frac{\theta_{\text{wall}}-\theta_{\text{cone}}}{R_{\text{wall}}-R_{\text{cone}}}(r-R_{\text{cone}}), \tag{1}$$

where u_{axial} is the measured axial inlet velocity, θ is the flow angle in the axial-radial direction, and θ_{cone} and θ_{wall} are the angles of the runner cone and the diffuser cone wall, respectively. r is the radial coordinate from the runner axis and R_{cone} is the runner cone radius. Equation (1) represents the low level of the radial velocity. The high level of the radial velocity is set to zero, an assumption used by many participants of the first workshop:

$$u_{\text{radial}}=0. \tag{2}$$

3.1.3 Surface Roughness. The organizers prescribed a surface roughness $k_s=10\ \mu$m (equivalent sand roughness height) for the entire draft tube. For the factorial design, a surface roughness of 0 and 200 μm were chosen. The upper limit corresponds to the roughness of cast iron [10].

Since wall functions are used to model the near-wall region, the surface roughness modifies the constant B in the assumed logarithmic velocity profile [11]:

$$\frac{U}{u_\tau}=\frac{1}{\kappa}\ln\left(\frac{yu_\tau}{\nu}\right)+B_{\text{smooth}}-\Delta B, \tag{3}$$

where $u_\tau=\sqrt{\tau_w/\rho}$, y, and ν represent, respectively, the friction velocity, the distance from the wall, and the kinematic viscosity. τ_w is the wall shear stress and ρ the density. The extra constant ΔB is added to account for the surface roughness effect. The CFD code used to perform the simulations, CFX 4.4 from AEA Technology, uses $\kappa=0.42$, $B_{\text{smooth}}=5.45$, and the correlation suggested by White for ΔB [11]:

$$\Delta B=\frac{1}{\kappa}\ln(1+0.3k_s^+),$$
$$k_s^+=\frac{k_s u_\tau}{\nu}. \tag{4}$$

The curve fit of Eq. (4) represents experimental data approximately for the smooth, transitional and fully rough regimes. In the limit of fully rough conditions, where viscous effects are negligible, Eq. (3) becomes

$$\frac{U}{u_\tau}=\frac{1}{\kappa}\ln\left(\frac{y}{k_s}\right)+8.3, \tag{5}$$

where Eq. (4) has been used.

3.1.4 Grid. The two grids used in the calculations have been produced by Bergström [7] using the program ICEM CFD. The coarse grid, shown in Fig. 3, is composed of 326,536 cells. It has a minimum angle of 37.6 deg and 284 cells have an angle lower

Table 1 Factorial design of the Turbine-99 test case

Run	1	2	3	4	5	6	7	8	9	10	11	12	13	14	15	16
TLS	−	+	−	+	−	+	−	+	−	+	−	+	−	+	−	+
RV	−	−	+	+	−	−	+	+	−	−	+	+	−	−	+	+
SR	−	−	−	−	+	+	+	+	−	−	−	−	+	+	+	+
Grid	−	−	−	−	−	−	−	−	+	+	+	+	+	+	+	+

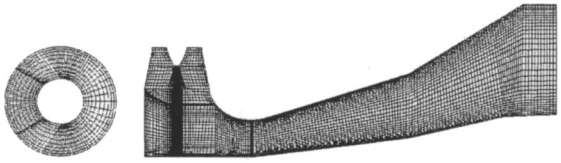

Fig. 3 Inlet and XZ midplane of the draft tube with the coarse grid

than 40 deg. The fine grid, shown in Fig. 4, has 668,166 cells. The minimum angle is 37.9 deg and 16 cells have an angle lower than 40 deg.

The grids have the same topology, and the refinement is general. The region below the cone is dense in order to resolve the separation zone. The near-wall cell size is determined by the requirement for the y^+ value at the cell center to be valid for the wall function method. The large and complex computational domain makes the requirement for the y^+ value at the cell center difficult to reach. The average value of y^+ for the 16 runs is 254 and the average standard deviation 231. A summary of the levels used for the different factors is presented in Table 2.

3.2 Other Computational Input. Several other input parameters were also required for the simulations.

3.2.1 Numerics. The code CFX 4.4 from AEA Technology was used for the simulations. The code is based on the finite-volume method and uses a colocated multiblock grid. More details concerning the code may be found in Ref. [12].

The standard k-ϵ model with the standard wall function was chosen to perform the isothermal, incompressible, and steady calculations. The choice of the turbulence model is motivated by the results of the first workshop, which showed no significant difference between different models. The standard k-ϵ model uses the eddy viscosity hypothesis for the Reynolds stresses, which relates them linearly to the mean velocity gradient:

$$-\overline{u_i u_j} = 2\nu_T S_{ij} - \tfrac{2}{3}k\delta_{ij}, \tag{6}$$

where ν_T is the eddy viscosity and S_{ij} is the mean strain rate tensor. The turbulent kinetic energy and its dissipation rate are used to get the velocity and length scales for the eddy viscosity, which is

$$\nu_T = C_\mu \frac{k^2}{\epsilon}. \tag{7}$$

The steady and incompressible equations for k and ϵ are

$$U_j \frac{\partial k}{\partial x_j} = -\overline{u_i u_j}\frac{\partial U_i}{\partial x_j} - \epsilon + \frac{\partial}{\partial x_j}\left[(\nu + \nu_T/\sigma_k)\frac{\partial k}{\partial x_j}\right], \tag{8}$$

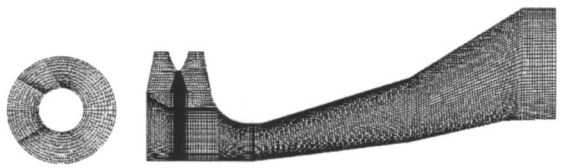

Fig. 4 Inlet and XZ midplane of the draft tube with the fine grid

Table 2 High and low levels of the factors

Factor/Level	−	+
Dissipation length scale (mm)	5	100
Radial velocity	Eq. (1)	Eq. (2)
Surface roughness (μm)	0	200
Grid	Coarse	Fine

Table 3 Differencing schemes [HUW, higher-order upwind differencing (2nd order); CENTRAL, central differencing (2nd order); HYBRID, hybrid differencing (1st order)], under-relaxation factors and solvers (BLST, Block Stone's method; ICCG, preconditioned conjugate gradients) used in the simulations

Equation	Differencing scheme	Under-relaxation factor	Linear solver
u velocity	HUW	0.65	BLST
v velocity	HUW	0.65	BLST
w velocity	HUW	0.65	BLST
pressure	CENTRAL	1	ICCG
k	HYBRID	0.70	LINE SOLVER
ϵ	HYBRID	0.70	BLST

$$U_j \frac{\partial \epsilon}{\partial x_j} = -C_{\epsilon 1}\frac{\epsilon}{k}\overline{u_i u_j}\frac{\partial U_i}{\partial x_j} - C_{\epsilon 2}\frac{\epsilon^2}{k} + \frac{\partial}{\partial x_j}\left[(\nu + \nu_T/\sigma_\epsilon)\frac{\partial \epsilon}{\partial x_j}\right], \tag{9}$$

where the summation convention is assumed and the model constants are: $C_\mu = 0.09$, $C_{\epsilon 1} = 1.44$, $C_{\epsilon 2} = 1.92$, $\sigma_k = 1$, and $\sigma_\epsilon = 1.3$.

The differencing schemes, under-relaxation factors, and solver methods for the linearized equations used for the computations are reported in Table 3. The choice of a first-order accurate scheme for the k and ϵ equations is motivated by the industrial nature of the flow.

3.2.2 Boundary Conditions. The experimental boundary conditions at the inlet of the draft tube provided by the organizers for the T mode, i.e. the top of the propeller curve, were used. The axial and tangential velocity mean components (u,w) were measured along a radial line. The radial velocity was specified as described above. The periodic fluctuations arising from the blade passages and the turbulent fluctuations in the measurements were both chosen by the organizers to contribute to the steady turbulent quantities ($\overline{u'^2}$, $\overline{v'^2}$ and $\overline{u'v'}$). The following assumptions at the inlet of the draft tube were made to perform the calculations as specified by the organizers:

$$\overline{v'^2} = \overline{w'^2},$$

$$\overline{u'v'} = \overline{v'w'} = \overline{u'w'},$$

where u', v', and w' represent the axial, radial, and tangential velocity fluctuations, respectively. The inlet conditions are assumed to be axisymmetric. At the outlet, the Neumann boundary conditions are imposed on all transport variables. Their gradient is set to zero except for the velocity gradient, which is modified to ensure mass conservation. Such an assumption is disputable, since the outlet is close to the straight diffuser where the flow still develops. Such a geometry was provided by the organizers of the first workshop. The pressure is extrapolated from upstream.

4 Results and Discussion

The engineering quantities used at the Turbine-99 workshops were used to evaluate the influence of the four input parameters:

- Wall pressure recovery:

$$C_{pw} = \frac{p_{\text{outlet wall}} - p_{\text{inlet wall}}}{\frac{1}{2}\rho(Q/A_{\text{inlet}})^2}.$$

- Mean pressure recovery:

$$C_{pm} = \frac{(1/A_{\text{outlet}})\int_{A_{\text{outlet}}} p\, dA - (1/A_{\text{inlet}})\int_{A_{\text{inlet}}} p\, dA}{(1/A_{\text{inlet}})\int_{A_{\text{inlet}}} \frac{1}{2}\rho(u^2+u^2+w^2)dA}.$$

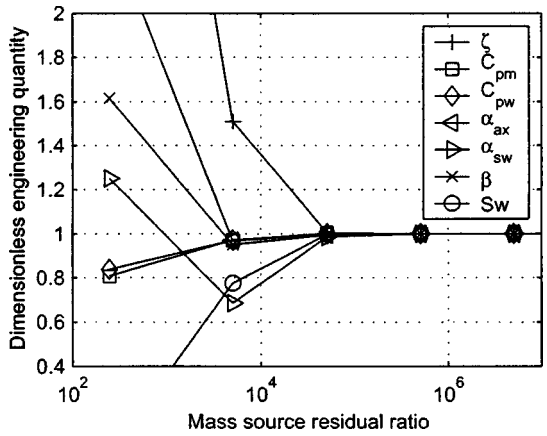

Fig. 5 Normalized engineering quantity function of the ratio of the mass source residual of the second iteration and the last iteration for run 2

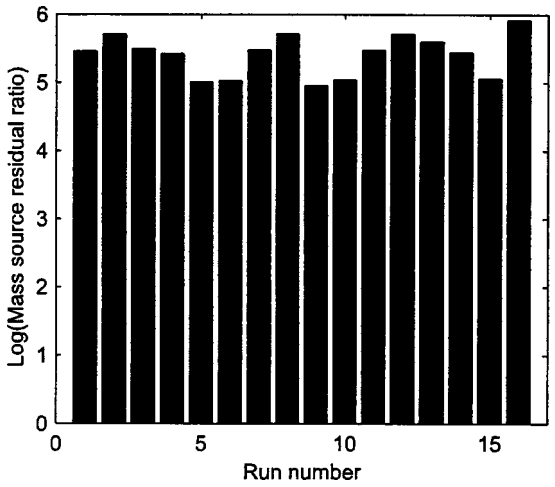

Fig. 6 Ratio of the mass source residual of the second iteration and the last iteration for the different runs

- Energy loss factor:

$$\zeta=\frac{\int_{A_{\text{inlet}}}E\vec{u}\cdot\vec{n}dA+\int_{A_{\text{outlet}}}E\vec{u}\cdot\vec{n}dA}{\int_{A_{\text{inlet}}}[\frac{1}{2}\rho(u^2+v^2+w^2)]\vec{u}\cdot\vec{n}dA},$$

where E represents the mechanical energy:

$$E=p+\tfrac{1}{2}\rho(u^2+v^2+w^2).$$

- Kinetic energy correction factor:

$$\alpha_{\text{axial}}=\frac{1}{A\overline{u^3}}\int_A u^3dA.$$

- Kinetic energy correction factor:

$$\alpha_{\text{swirl}}=\frac{1}{A\overline{u^3}}\int_A w^2udA.$$

- Momentum correction factor:

$$\beta=\frac{1}{A\overline{u^2}}\int_A u^2dA.$$

- Swirl intensity:

$$\text{Sw}=\frac{1}{R}\frac{\int_A ruw\,dA}{\int_A u^2dA},$$

where $\vec{u}$ is the velocity vector with the axial, radial, and tangential components u, v, and w, respectively. Q is the volume flow rate, p is the static pressure, ρ is the density, and A is the cross-section area with the outward normal vector $\vec{n}$. α_{axial}, α_{swirl}, β, and Sw are evaluated at cross section III, which is midway between the end of the elbow and the outlet of the draft tube (see Fig. 1). The center of the cross section is used as the origin for the calculation of α_{sw}, Sw, and r.

4.1 Convergence Criteria and Iterative Error. In order to reduce the computational time without losing accuracy, an investigation of the iterative error as a function of the mass source residual was undertaken on runs 2, 4 and 8. Figure 5 represents the engineering quantities as a function of the ratio of the mass source residual obtained at the second and the last iteration for run 2. The values are normalized with the value obtained at the highest ratio of the mass source residual, i.e., 7.1×10^8. The solution is assumed fully converged for this residual. The iterative error for the engineering quantities becomes lower than 2% for a mass source residual of 10^5. The result is similar for runs 4 and 8 (see Table 4). Therefore, the convergence criterium was set to 10^5 for all runs, assuming the iterative error is independent of the run. Convergence was easily achieved independently of the levels of the input parameters. The ratio of the mass source residual of the second to the last iteration for the different runs is represented in Fig. 6. The average residual reduction for the u, v, and w equations was above four decades, while for the k and ϵ equations above five decades.

The convergence criterion induces an iterative error on the statistics. A confidence interval for each statistic is necessary to determine whether an effect is significant. The iterative errors evaluated for runs 2, 4, and 8 are used to calculate the dimensionless sample standard deviation s for each engineering quantity:

$$s^2=\frac{\Sigma_{i=2,4,8}e_i^2}{2}, \tag{10}$$

where e_i is the iterative error of the ith run. The standard normal deviate

$$t=\frac{y_0-\eta}{s} \tag{11}$$

is considered, where y_0 is the dimensionless limit of the confidence interval and η the dimensionless mean value of the differ-

Table 4 Iterative error in percent for runs 2, 4, and 8 with a mass source residual of 10^5. Sample standard deviations and limits for a 95% confidence interval.

	C_{pw}	C_{pm}	ζ	α_{ax}	α_{sw}	β	Sw
Run 2	0.01	0.06	0.15	0.34	1.32	0.57	0.30
Run 4	0.04	0.05	0.11	0.58	0.29	0.23	0.16
Run 8	0.22	0.32	1.08	0.44	1.86	0.35	0.60
s	0.02	0.06	0.60	0.32	2.65	0.25	0.24
y_0	0.68	1.01	3.35	2.45	7.00	2.17	2.10

Table 5 Mean value of the engineering quantities for runs 1 to 16

Run	1	2	3	4	5	6	7	8
C_{pw}	1.084	1.089	0.994	1.013	1.047	1.058	0.965	0.985
C_{pm}	0.948	0.943	0.810	0.828	0.916	0.920	0.782	0.799
ζ	0.054	0.050	0.190	0.163	0.080	0.072	0.215	0.195
α_{ax}	1.144	1.219	0.876	1.352	1.186	1.232	1.044	1.408
α_{sw}	0.234	0.090	0.057	0.062	0.206	0.086	0.070	0.066
β	1.372	1.215	0.987	1.240	1.331	1.207	1.111	1.281
Sw	0.268	0.160	0.149	0.082	0.240	0.157	0.152	0.081
Run	9	10	11	12	13	14	15	16
C_{pw}	1.089	1.088	0.991	1.016	1.032	1.062	0.969	0.983
C_{pm}	0.950	0.945	0.809	0.828	0.903	0.917	0.786	0.799
ζ	0.046	0.050	0.189	0.165	0.096	0.071	0.218	0.194
α_{ax}	1.170	1.160	0.968	1.380	1.081	1.371	1.071	1.350
α_{sw}	0.194	0.083	0.058	0.065	0.246	0.103	0.093	0.062
β	1.324	1.170	1.051	1.257	1.323	1.300	1.157	1.248
Sw	0.239	0.159	0.133	0.082	0.270	0.163	0.174	0.083

ences between the fully converged solution and the solution with a mass source residual of 10^5 for the different runs. The differences between the fully converged and partially converged solution are expected to be normally distributed around zero; thus $\eta=0$. The quantity t is assumed to have a Student's t distribution [6]. For a confidence interval of 95% with two degrees of freedom $t=2.920$. The limits are reported in Table 4.

4.2 Results of Factorial Design. The engineering quantities were calculated for the 16 runs. The results are reported in Table 5. The results of the main and joint effects are reported in percent of the mean value in Table 6. For instance, the main effect of the turbulence length scale on the energy loss factor ζ is calculated as

$$\zeta_{\mathrm{TLS}}=\frac{\zeta_2+\zeta_4+\zeta_6+\zeta_8+\zeta_{10}+\zeta_{12}+\zeta_{14}+\zeta_{16}}{8}-\frac{\zeta_1+\zeta_3+\zeta_5+\zeta_7+\zeta_9+\zeta_{11}+\zeta_{13}+\zeta_{15}}{8}.$$

The joint effect of the turbulence length scale and the radial velocity on ζ is

$$\zeta_{\mathrm{TLS}\times\mathrm{RV}}=\frac{\zeta_1+\zeta_4+\zeta_5+\zeta_8+\zeta_9+\zeta_{12}+\zeta_{13}+\zeta_{16}}{8}-\frac{\zeta_2+\zeta_3+\zeta_6+\zeta_7+\zeta_{10}+\zeta_{11}+\zeta_{14}+\zeta_{15}}{8}.$$

Some effects are disregarded due to the iterative error. These effects are outside the confidence interval of 95%. Significant effects deviate from the normal distribution on a normal probability plot. See Fig. 7 for the effects on the energy loss factor.

The function of a draft tube is to recover the kinetic energy leaving the runner into pressure with a minimum of losses. Therefore, the pressure recovery coefficients are of major interest. Pressure recovery (C_{pw}) based on wall pressure is used for comparison with the experimental value. The mean value of the 16 runs is 1.029 and this should be compared with the experimental value of 1.12. Pressure recovery (C_{pm}) based on the mean values of the pressure over the inlet and outlet areas may be, however, more relevant when evaluating the performance of the draft tube, since it is less sensible to local variations. Both pressure recovery factors are mostly influenced by the radial velocity, a parameter not measured for the workshop. A small separation zone is present below the runner cone at the low level of the radial velocity. The high level of the radial velocity induces a large separation zone from the runner cone to the elbow. It strongly alters the flow structure and increases the energy loss factor. Both pressure recovery factors decrease with a zero radial velocity. This result is confirmed with the approximate analytical relation between C_{pm} and ζ found using the energy equation:

$$\zeta\approx\left(1-\frac{C_{pm}}{\alpha_{\mathrm{inlet}}}\right)-\frac{\alpha_{\mathrm{outlet}}}{\alpha_{\mathrm{inlet}}}\left(\frac{A_{\mathrm{inlet}}}{A_{\mathrm{outlet}}}\right)^2,$$

where α_{outlet} and α_{inlet} represent the total kinetic energy correction factors. Both terms in parentheses are of the same order, around 0.1. As $C_{pm}\approx 1$, a small variation in the pressure recovery induces a large variation of the loss factor. It explains the effect of 49% on ζ as the radial velocity profile moves from its low level, attached flow, to its high level, zero radial velocity.

The surface roughness has a lower influence on the loss factor than expected, 11%. From pipe flow, it is known that an increase in surface roughness from 0 to 200 μm corresponds to an increase of the friction factor by 56% at the inlet and 16% at the outlet, at the corresponding Reynolds numbers. The effects of surface roughness do not influence the flow as it does in fully developed pipe flow. More surprising is the small influence of the turbulence length scale on ζ, around 6% despite a factor 20 between the high and low levels.

The difference between the two grids does not have a striking influence on the engineering quantities relative to the other factors. This shows that the present grid refinement is not significant enough to improve the accuracy of the engineering quantities.

Table 6 Mean value of the engineering quantities for the 16 runs. Main and joint effects (E=ABC, F=ABD, G=BCD and H=ABCD) in percent of the factors (A=TLS, B=RV, C=SR and D=grid) on the engineering quantities, significant values are in bold. Joint effects BCD and ABCD are negligible and not presented.

	Mean	A	B	C	D	AB	AC	AD	BC	BD	CD	E	F	G	H
C_{pw}	1.029	**1**	**−4**	**−2**	0	0	0	0	0	0	0	0	0	0	0
C_{pm}	0.868	1	**−7**	**−2**	0	0	0	0	0	0	0	0	0	0	0
ζ	0.128	**−6**	**49**	**11**	1	−3	−1	−1	0	−2	0	2	1	−1	0
α_{ax}	1.188	**10**	−1	2	−2	**6**	0	−1	1	2	−2	**−3**	0	0	0
α_{sw}	0.111	**−30**	**−40**	5	2	**28**	−3	−5	1	−5	−2	−2	**7**	−1	2
β	1.223	1	**−5**	2	−1	**6**	0	−1	1	0	−1	−2	1	0	0
Sw	0.162	**−25**	**−28**	2	1	**4**	−2	−1	2	**−3**	0	−2	**4**	0	1

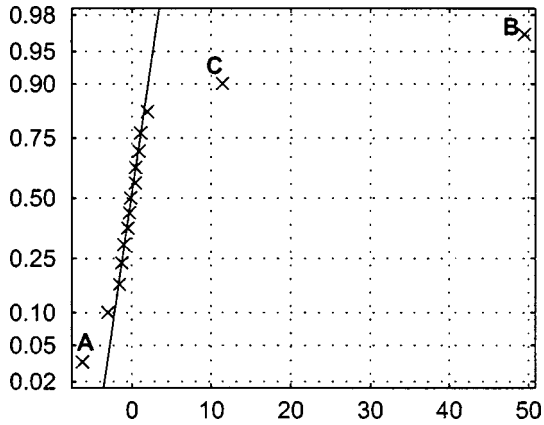

Fig. 7 Normal probability plot for the effects on ζ. Significant effects deviate from the normal distribution represented by the straight line.

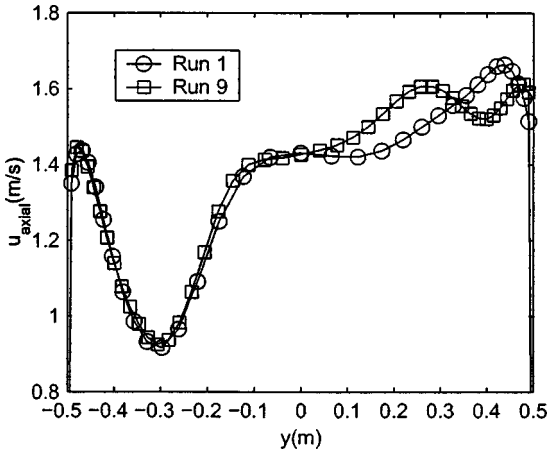

Fig. 8 Horizontal velocity profiles at the center of cross section II for runs 1 and 9

Such a result does not mean that the solution is grid independent as seen in Fig. 8, where the axial velocity profiles of runs 1 and 9 at cross section II show some differences. The weak sensitivity of the engineering quantities to the grid is due to their integral form, which suppresses local deviations. A Richardson extrapolation may be performed to estimate the error due to the space discretization. Bergström and Gebart [4] estimated the grid error to 3–7% for the wall pressure recovery and a grid with 3.9×10^6 to 222 $\times10^6$ cells to lower the grid error to 1% for C_{pw}, using a Reynolds stress model. Such a topology extends beyond our computational power and had to be disregarded. Thus, future efforts should focus on a better estimate of the radial velocity rather than a further grid refinement, because the radial velocity has a much stronger influence on the engineering quantities.

Several joint effects appear, for instance, the interaction between the turbulence length scale and the radial velocity for α_{swirl}, which is the contribution to the kinetic energy flux from the tangential velocity. The flow field in cross section III is shown in Fig. 9 for runs 1–4. These are the runs calculated with the coarse grid and represent the four different combinations of the turbulence length scale and radial velocity levels. The streamwise velocity field is indicated with contours and the secondary motion is described by vectors. It is obvious that both parameters have a significant influence on the flow. The large vortex to the left moves further to the left when the turbulence length scale is increased from 5 to 100 mm (top row to bottom row). Less energy is dissipated with a high turbulence length scale between the inlet and the beginning of the elbow than with a low turbulence length scale. Thus, the swirl intensity is higher, and the gyroscopic effect displaces the vortex further to the left. When the radial velocity is changed from the low level [Eq. (1)] to the high level ($u_{\text{radial}}=0$), a new counterrotating vortex appears to the right (left column to right column). For the high level of the radial velocity, a large separation zone from the runner cone to the elbow appears. The separation zone splits into two vortices, one due to the gyroscopic effect and one due to the fluid impinging on the bottom of the draft tube. These effects are confirmed in Table 6, where α_{swirl} decreases when either the turbulence length scale or the radial velocity changes from low to high level. However, there is also a strong interaction effect (28%). The interpretation is that the effect

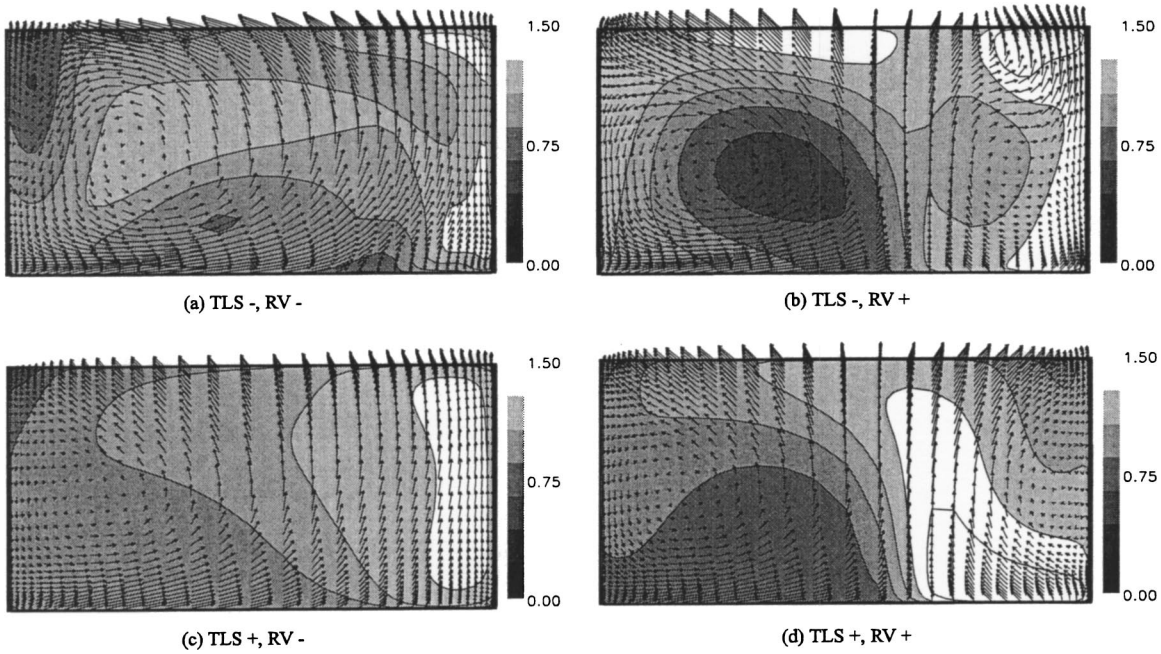

Fig. 9 Streamwise velocity (contours) and secondary motion (vectors) in cross section III. View is upstream: (a) run 1, (b) run 3 (c) run 2, (d) run 4.

of increasing the turbulence length scale is different, depending on the level of the radial velocity. Since the joint effect is positive, α_{swirl} increases more when the turbulence length scale is increased at a high level of radial velocity, than it does at a low level.

Assuming a Student's t distribution for the 16 runs, a 95% confidence interval for the wall pressure recovery was calculated, $C_{pw}=1.029\pm0.096$. The present confidence interval does not include the grid error (3–7%) and the iterative error (<2%). Therefore, the input parameters analyzed here, the iterative error and grid error explain partially the scatter in the results of the first Turbine-99 workshop (see Fig. 2). The rest of the explanation may be found in the results of the second workshop, where a reference simulation was performed by all participants with the boundary conditions, the grid, and the turbulence model specified. The purpose was to resolve the differences in implementation and postprocessing between different contributors. The results still show a large scatter for the wall pressure recovery, $0.86\leqslant C_{pw}/C_{pw}^{\text{mean}}\leqslant1.38$. When submitted data were recalculated with the same method, the scatter decreased, $0.87\leqslant C_{pw}/C_{pw}^{\text{mean}}\leqslant1.28$. Obviously, postprocessing is an important issue for workshops and engineers. The mean pressure (C_{pm}) recovery was also calculated by the organizers with the data from the participants, $0.95\leqslant C_{pm}/C_{pm}^{\text{mean}}\leqslant1.06$. Unfortunately, this factor was not requested for the workshops. Nevertheless, it points out the difficulty to calculate C_{pw} correctly.

4.3 Discussion. Factorial design applied to CFD yields a confidence interval for any engineering quantity, where the effects of all input parameters under investigation are included. This interval, together with the iterative and grid errors, gives a measure of the uncertainty of the numerical simulation. The method also shows which parameter has the largest influence and which parameters interact significantly. Therefore, a deeper understanding of the flow and valuable insight for further investigations may be reached. An important benefit of the method is the possibility to choose both variable parameters, as in the Turbine-99 example, and categorical parameters such as the turbulence model or discretization scheme. For instance, an interaction effect could be the response of different turbulence models to different levels of dissipation at the inlet.

The major challenge is the choice of parameters and their high and low levels. Procedures to find parameters and appropriate levels were shown in the Turbine-99 example. Another challenge, specific to the application to CFD, is the significance level for an effect. Experimental runs are always associated with a random error, which defines a significance threshold for each effect. If the effect is below the threshold, it is assumed to be noise. There are no natural, significant random errors in CFD. The iterative error was used here to define a threshold and therefore some effects were assumed to be insignificant. By allowing a non-negligable iterative error, simulation time was decreased substantially.

With factorial design the engineer has a systematic, objective, and quantitative method to evaluate the sensitivity to different input parameters. A large main effect will identify, e.g., an important boundary condition for which further analysis or experiments have to be considered. Therefore, the results form a reliable foundation for crucial decisions. The increased computational time resulting from the larger number of simulations may be warranted for large investments or safety critical projects.

Factorial design may also be used to organize workshops where several scientists with different affiliations contribute with one or more runs. However, the results of both Turbine-99 workshops show that workshops are a difficult exercise, as discussed by Apsley and Leschziner [13]. Even if most of the inputs are defined by the organizers, there are still some degrees of freedom leading to discrepancies between the results due to preprocessing, codes, and postprocessing.

As the computational power increases, factorial design may be automated and implemented in commercial codes, where the engineer will select the levels for the desired inputs. The program will perform the different simulations and present the different engineering quantities with a confidence interval as well as the main and joint effects.

5 Conclusion

The application of factorial design to CFD has been discussed. It is a systematic, objective, and quantitative method to investigate the influence of input parameters, such as unknown boundary conditions, turbulence models, and computational grids. The main task is the choice of parameters and their levels.

The illustration of the method with the Turbine-99 test case, a hydropower draft tube flow, clearly illustrates the advantages. Engineering quantities are given within a confidence interval based on the influence of all parameters. Main and joints effects of input parameters are evaluated and permit a better understanding of the flow. For instance, the radial velocity is shown to be a fundamental factor for obtaining accurate results of the pressure recovery and especially the energy loss factor of a draft tube. The use of factorial design in engineering applications may improve the quality of the results and increase the trust in CFD in the industry.

References

[1] Hirsh, C., 2001, "The QNET-CFD Project," QNET-CFD Network Newsletter, **1**, January, pp. 4–5.

[2] Hutton, A. G., and Casey, M. V., 2001, "Quality and Trust in Industrial CFD—A European Initiative," 39th Aerospace Sciences Meeting and Exhibit, Reno, NV, Jan. 8–11.

[3] Casey, M., and Wintergerste, T., eds., 2000, *Best Practice Guidelines*, ERCOFTAC Special Interest Group on Quality and Trust in industrial CFD.

[4] Bergström, J., and Gebart, B. R., 1999, "Estimation of the Numerical Accuarcy for the Flow Field in a Draft Tube," Int. J. Numer. Methods Heat Fluid Flow, **9**, pp. 472–486.

[5] Iaccarino, G., 2000, "Prediction of the Turbulent Flow in a Diffuser With Commercial CFD Codes," Center for Turbulence Research, Annual Research Briefs, pp. 271–278.

[6] Box, E. P., Hunter, W. G., and Hunter, J. S., 1978, *Statistics for Experimenters*, Wiley, New York.

[7] Gebart, B. R., Gustavsson, L. H., and Karlsson, R. I., 1999, Proceedings of Turbine-99 Workshop on Draft Tube Flow, Porjus, Sweden, June 20–23.

[8] Karlsson, R. I., and Gustavsson, L. H., 2001, The Second ERCOFTAC Workshop on Draft Tube Flow, Älvekarleby, Sweden, June 18–20, published at http://www.luth.se/depts/mt/strl/turbine99/.

[9] Dahlbäck, N., 1996, "Redesign of Sharp Heel Draft Tube—Results From Tests in Model and Prototype," Proc. of the XVIIIth IAHR Symp. on Hydraulic Machinery and Cavitation, Vol. 2, pp. 985–993.

[10] Roberson, J. A., and Crowe, C. T., 1997, *Engineering Fluid Mechanics*, Wiley, New York, p. 368.

[11] White, F. M., 1991, *Viscous Fluid Flow*, McGraw-Hill, New York, pp. 426–428.

[12] AEA Technology, "CFX4.4 Solver," Fluid Dynamics Services, Building 8.19, Harwell Laboratory, Oxfordshire, United Kingdom.

[13] Apsley, D. D., and Leschziner, M. A., 1999, "Advanced Turbulence Modelling of Separated Flow in a Difffuser," Flow, Turbul. Combust., **63**, pp. 81–112.